Field-dependent antiferromagnetism and ferromagnetism of the two copper sublattices in $Sr_2Cu_3O_4Cl_2$

M. A. Kastner
Center of Materials Science and Engineering, Massachusetts Institute of Technology, Cambridge, Massachusetts 02139

Amnon Aharony
Center of Materials Science and Engineering, Massachusetts Institute of Technology, Cambridge, Massachusetts 02139 and School of Physics and Astronomy, Raymond and Beverly Sackler Faculty of Exact Sciences, Tel Aviv University, Tel Aviv 69978, Israel

R. J. Birgeneau and F. C. Chou
Center of Materials Science and Engineering, Massachusetts Institute of Technology, Cambridge, Massachusetts 02139

O. Entin-Wohlman
School of Physics and Astronomy, Raymond and Beverly Sackler Faculty of Exact Sciences, Tel Aviv University, Tel Aviv 69978, Israel

M. Greven
Center of Materials Science and Engineering, Massachusetts Institute of Technology, Cambridge, Massachusetts 02139

A. B. Harris
Department of Physics, University of Pennsylvania, Philadelphia, Pennsylvania 19104

Y. J. Kim, Y. S. Lee, and M. E. Parks
Center of Materials Science and Engineering, Massachusetts Institute of Technology, Cambridge, Massachusetts 02139

Q. Zhu
Department of Physics, Brookhaven National Laboratory, Upton, New York 11973

(Received 2 October 1998)

The Cu_3O_4 layer in $Sr_2Cu_3O_4Cl_2$ is a variant of the square CuO_2 lattice of the high-temperature superconductors, in which the center of every second plaquette contains an extra Cu^{2+} ion. The ions that make up the conventional CuO_2 network, called CuI, have CuI-CuI exchange energy ≈ 130 meV, and order antiferromagnetically at about 380 K; the CuII-CuII exchange is only ≈ 10 meV, and the CuII's order at ≈ 40 K. A study is reported here of the dependence of the magnetization on field, temperature, and crystallographic orientation for this interesting system. We show that the small permanent ferromagnetic moment, that appears when the CuI spins order, and the unusual spin rotation transitions seen most clearly for one particular direction of the magnetic field, are the result of several small bond-dependent anisotropic terms in the spin Hamiltonian that are revealed because of the frustration of the isotropic Heisenberg interaction between CuI and CuII spins. These include a term which favors collinearity of the CuI and CuII spins, which originates from quantum fluctuations, and also the pseudodipolar interaction. Some of these small interactions also come into play in other lamellar cuprates, connected with the high-T_c superconductivity materials, and in many spin-chain and spin-ladder compounds. [S0163-1829(99)03218-X]

I. INTRODUCTION

The explosion of experimental and theoretical work triggered by the discovery of high-temperature superconductivity has led to great progress in our understanding of quantum magnetism. In particular, the essential component of materials such as La_2CuO_4, a high-T_c superconductor when doped with Sr or excess oxygen, is the two-dimensional (2D) CuO_2 layer consisting of a square lattice with Cu ions on the corners and O ions on the edges. Since the copper ions have electronic configuration d^9 they have spin $S=1/2$; the interaction between nearest-neighbor spins is well described by the Heisenberg model. In the past few years symbiotic experimental and theoretical studies of materials containing CuO_2 layers have provided a quantitative understanding of the 2D $S=1/2$ square lattice Heisenberg quantum antiferromagnet (SLHQA).[1] However, the atomic arrangements of Cu and oxygen in multielement copper oxides show remarkable variability. In addition to the CuO_2 layer one finds Cu-O chains and ladders. The latter have lately been the subject of great interest because the quantum magnetism is predicted to be extraordinarily sensitive to the number of chains in a ladder.[2]

Recently, interesting results have emerged for a novel variant of the CuO_2 layer, contained in the compounds $Sr_2Cu_3O_4Cl_2$ and $Ba_2Cu_3O_4Cl_2$ (2342). In these materials every second square of the CuO_2 lattice contains an addi-

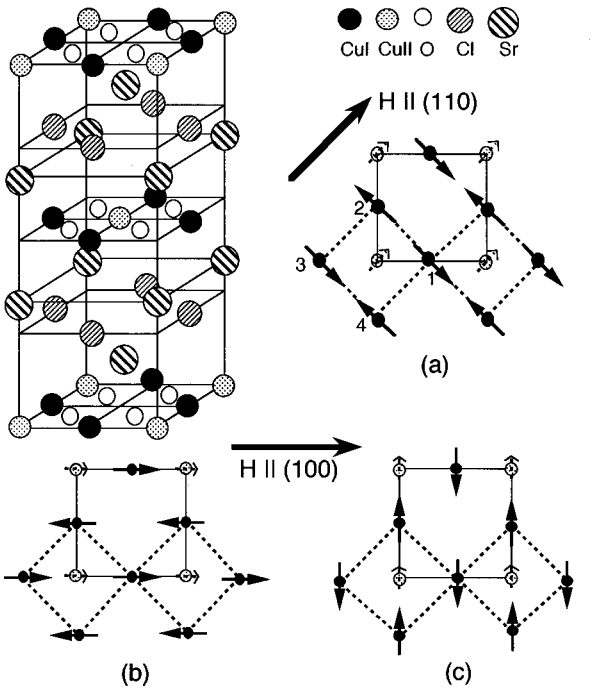

FIG. 1. Structure of $Sr_2Cu_3O_4Cl_2$ and of the Cu_3O_4 layer, including spin configurations for (a) $\mathbf{H}\|(110)$, (b) $\mathbf{H}\|(100)$, and $H_{c1}<H<H_{c2}$, and (c) $\mathbf{H}\|(100)$ and $H_{c2}\ll H$. The figure shows only the part of $\mathbf{M}_{\mathrm{II}}$ induced by the internal pseudodipolar field $-4J_{\mathrm{pd}}\hat{\Gamma}\mathbf{M}_{\mathrm{I}}^{\dagger}$. There also exists an additional small canting of the CuI moments in cases (a) and (c), and a nonzero H induces a large component of $\mathbf{M}_{\mathrm{II}}$ along $\mathbf{H}$ in case (c) (not shown).

tional Cu^{2+} ion in its center, creating two interpenetrating square lattices of Cu ions (see Fig. 1).[3,4] The Cu ions forming the conventional CuO_2 layer (CuI's) have a very large CuI-CuI antiferromagnetic coupling ($J_0=130$ meV), similar to that in the high-T_c parent compounds. Together with the weak interplanar coupling, these yield three-dimensional antiferromagnetic order at a Néel temperature T_I near 380 K. Since the Cu d^9 ions at the center of the squares (CuII's) are surrounded by four equidistant CuI neighbors, the isotropic Heisenberg interaction between CuI and CuII spins is frustrated. Thus, the two Cu sublattices are almost decoupled. The weaker CuII-CuII coupling then gives antiferromagnetic order at a separate lower Néel temperature $T_{\mathrm{II}}\approx 30-40$ K.[5–8] We have recently provided evidence that the CuII sublattice, similar to the CuI sublattice, behaves as a 2D $S=1/2$ SLHQA at temperatures well above T_{II}.[9] The critical behavior near this transition is that of the two-dimensional Ising model, resulting from the uniaxial anisotropy which comes from the CuI-CuII coupling (as explained below). This anisotropy is the result of an effective CuI-CuII interaction, which favors colinearity of the spins in the two subsystems. This term, which is absent in the mean field theory, results from quantum fluctuations.

One prominent feature of this system is a small ferromagnetic permanent ($H=0$) moment which appears at the Néel temperature of the CuI's. This ferromagnetism, corresponding to $\sim 10^{-3}\mu_B$ per CuI, cannot result from the Dzyaloshinsky-Moriya antisymmetric exchange,[5–8] because symmetry forbids such an effect in the perfectly tetragonal structure of $Sr_2Cu_3O_4Cl_2$ and $Ba_2Cu_3O_4Cl_2$. In a short publication[9] we have shown that the permanent moment arises instead from the pseudodipolar interaction between the spins of the CuI's and those of the CuII's. This results from the bond-dependent anisotropic CuI-CuII coupling.[9] Indeed, the near frustration of the coupling between the two kinds of Cu atoms has allowed us to determine several small terms in the spin Hamiltonian, in addition to the pseudodipolar interaction. These terms also arise in other Cu oxides. For example, the CuII-CuII nearest-neighbor interaction, resulting from superexchange through two oxygen atoms, is closely related to the second nearest-neighbor interaction in the CuO_2 layer of the high-T_c compounds. Furthermore, the anisotropic coupling between CuI and CuII ions in $Sr_2Cu_3O_4Cl_2$ also arises in the coupling between ladders in the spin-ladder compounds. Our measurements have also allowed us to determine the fourfold spin anisotropy energy of the CuI's, which arises in all the tetragonal cuprates. In this paper we provide a more complete description of the magnetization as a function of field and temperature in $Sr_2Cu_3O_4Cl_2$. After a description of experimental details in Sec. II, we present the results of our measurements of the spin rotation transitions in Sec. III. In Secs. IV and V we discuss the theories which provide excellent fits to the data for fields $H>0.1$ T and for temperatures $T_{\mathrm{I}}>T>T_{\mathrm{II}}$ and $T<T_{\mathrm{II}}$, respectively. The former generalizes the low-temperature approximation presented in Ref. 9. Finally, in Sec. VI we summarize our conclusions and point out some unresolved problems.

II. EXPERIMENTAL DETAILS

We have focused on the material $Sr_2Cu_3O_4Cl_2$ for which we have grown large single crystals by slow cooling from the melt. The structure of this material, as well as a sketch of the Cu_3O_4 layer, is shown in Fig. 1. Small crystals ~ 1 mm$\times 1$ mm$\times 0.5$ mm with the c axis (normal to the Cu_3O_4 layer) perpendicular to the large face are used for magnetization measurements with a Quantum Design SQUID magnetometer at fields up to 5.5 T.

High-resolution synchrotron x-ray powder diffraction measurements have been carried out at the National Synchrotron Light Source at Brookhaven National Laboratory. We find that the crystal remains perfectly tetragonal, space group $I4/mmm$, for temperatures $15<T<550$ K. The lattice constants are shown as a function of temperature in Fig. 2; at low $T<50$ K, they are $a=5.457$ Å and $c=12.52$ Å. The a lattice constant is independent of T below $T_{\mathrm{I}}\sim 325$ K, but begins to increase with T at higher T. The c lattice parameter is independent of T below ~ 50 K and increases with T at higher T. The latter also shows a kink at ~ 325 K. There is no feature that can be clearly identified with $T_{\mathrm{I}}\sim 380$ K where the CuI's order, with $T_{\mathrm{II}}\sim 40$ K where the CuII's order, or with 100 K where peculiar behavior of the very low field magnetization is observed, presumably related to antiferromagnetic domain wall motion.

III. PHENOMENOLOGICAL DISCUSSION OF THE MAGNETIZATION

Before presenting the theory we show that several qualitative features of the system can be deduced directly from

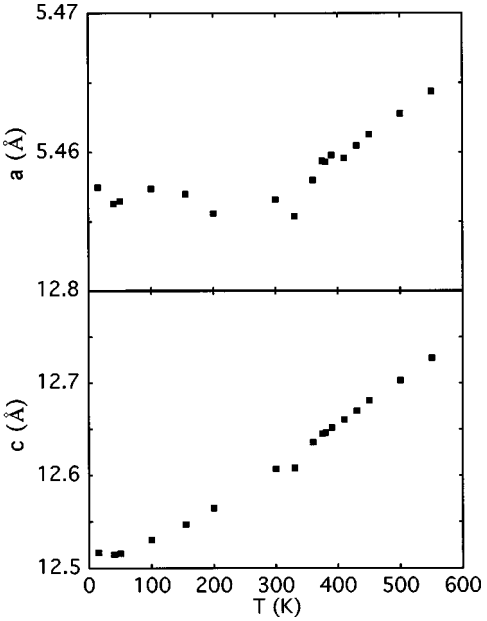

FIG. 2. Lattice constants as a function of temperature, measured using high reolution synchrotron x-ray scattering.

our measurements. Figure 3 shows the magnetic moment as a function of field at 200 K with the field applied in the (100) and (110) directions. In both cases there is a small permanent moment M_p, the extrapolation of $M(H)$ to $H=0$. This extrapolation depends on the range of H from which it is deduced: it grows with H at low field and saturates above $\sim 0.1-0.3$ T. No permanent moment is found for the field in the (001) direction (see inset of Fig. 3). For the (110) direction the susceptibility χ^{110} is independent of H from ~ 0.1 to 5 T and extapolation from any H in this range to $H=0$ gives the same value of M_p, which we call M_S^{110}. However, in the (100) direction the slope of $M(H)$ changes with H. In fact, at 200 K the $M(H)$ data in the (100) direction display two phase transitions, resulting, as discussed below, from rotation of the CuI staggered moment. At 200 K, these occur at the fields $H_{c1}\sim 0.3$ T and $H_{c2}\sim 1.8$ T. Between these two transition fields $M(H)$ is linear, with slope χ^{100}, smaller by about 10% than χ^{110}, and with an extrapolated permanent

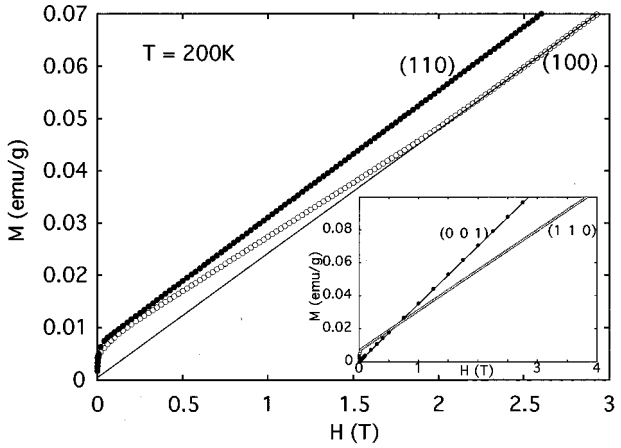

FIG. 3. Magnetic moment M vs H for $\mathbf{H}\|(110)$ and (100) at 200 K. The inset compares M for $\mathbf{H}\|(110)$ and $\mathbf{H}\|(001)$.

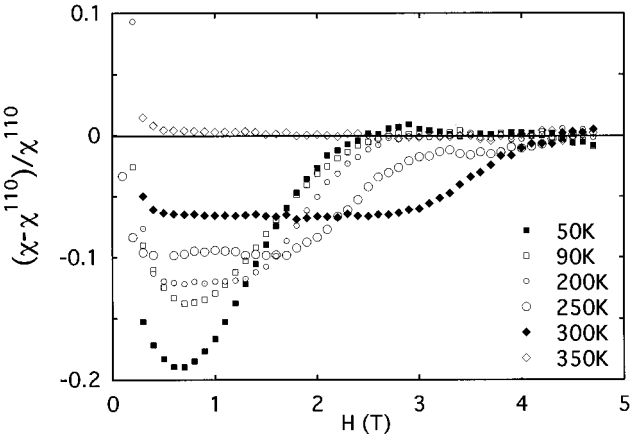

FIG. 4. Fractional deviation of $\chi=dM/dH$ for $\mathbf{H}\|(100)$ from the susceptibility in the (110) direction χ^{110}.

moment $M_S^{100}<M_S^{110}$. At high field the slope appears to approach χ^{110} and the value of M_p obtained from extrapolation of the high-H line to zero approaches zero, as illustrated by the solid line in Fig. 3. The phase transitions for $\mathbf{H}\|(100)$ can be identified quite clearly in Fig. 4, where we plot the fractional deviation of the susceptibility, $\chi=dM/dH$, in the (100) direction from its value in the (110) direction χ^{110} as a function of H. For 300, 250, and 200 K one observes the two transitions, between which there is a constant $\chi^{100}<\chi^{110}$. As the temperature is lowered these two transitions merge and disappear. At 90 K the susceptibilitiy has only a broad minimum near 0.8 T. By comparison with the theory, discussed below, we estimate that the phase transitions disappear below ~ 150 K.

The independence of the susceptibility on H for $\mathbf{H}\|(110)$, and the fact that this direction yields the largest values of χ and of M, identify (110) as the easy direction. For $T_{\mathrm{II}}<T<T_{\mathrm{I}}$, the CuI's are ordered antiferromagnetically and therefore their susceptibility is larger in the direction perpendicular to the staggererd moment. In that direction the moments can cant to give a transverse ferromagnetic moment even at zero temperature. We denote the CuI susceptibilities parallel and perpendicular to the staggered moment by $\chi_{\mathrm{I}\|}$ and $\chi_{\mathrm{I}\perp}$. In this range of T the CuII's are still not ordered, so they have an isotropic susceptibility χ_{II}. From these considerations we conclude that when the field is along (110) the spins must have the structure shown in Fig. 1(a), with $\chi^{110}\approx\chi_{\mathrm{II}}+2\chi_{\mathrm{I}\perp}$ (the factor 2 comes from the structure of the unit cell, with two CuI's per CuII). Indeed, the theory presented below confirms this conclusion, apart from small corrections which arise from the CuI-CuII coupling. The lower susceptibilities observed for fields in other directions must imply some mixture of $\chi_{\mathrm{I}\perp}$ and $\chi_{\mathrm{I}\|}$. We have proposed that the minimal susceptibility observed in the intermediate phase for the (100) direction, as illustrated by Fig. 4, results from the structure shown in Fig. 1(b), with $\chi^{100}\approx\chi_{\mathrm{II}}+2\chi_{\mathrm{I}\|}$. Indeed, this is also confirmed by our detailed theory presented below. The existence of the permanent moments in these two configurations implies the existence of some internal magnetic field, which prefers ordering of the CuII ferromagnetic moment perpendicular to the CuI staggered moment when the latter is in a (110) direction, and parallel to it when it is in the (100) direction. Our theory indeed predicts such a pseudodipolar field. This scenario is also supported by the

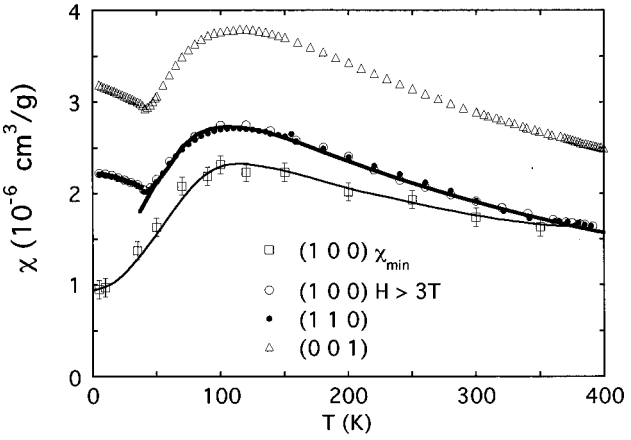

FIG. 5. Suceptibility vs T. For (110) and (001) χ is independent of H, as seen in Fig. 4. For the (100) direction the high field susceptibility and the minimum value of the susceptibility are both plotted. Above ~ 3 Tχ is isotropic in the plane and is well described by the 2D $S=1/2$ SLHQA model indicated by the heavy line through the data, as described in the text.

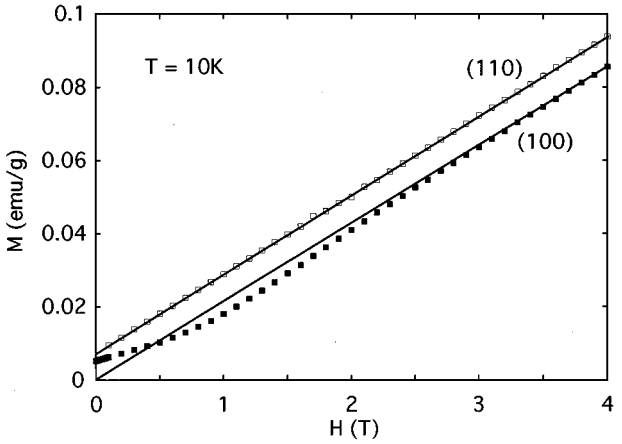

FIG. 6. $M(H)$ for $\mathbf{H}\|(100)$ and $\mathbf{H}\|(110)$ at $T=10$ K, well below the antiferromagnetic ordering temperature T_{II} of the CuII's.

behavior at very high $H(\ll J_0)$. The fact that the same susceptibility χ^{110} is observed for high H in *any* direction implies that in that limit the staggered moments become perpendicular to the field, as plotted for $\mathbf{H}\|(100)$ in Fig. 1(c), overcoming the anisotropy which causes them to prefer the (110) direction at low H.

Figure 5 shows the field-independent susceptibilities for the (001) and (110) directions and the high-field susceptibility for the (100) direction. We also plot the minimum value, $\chi_{\min}$, of $\chi(H)$ in the (100) direction, which corresponds to χ^{100} for temperatures where there are phase transitions. At high fields (>3 T) the susceptibility is the same in the (100) and (110) directions. The approximately temperature independent difference between the (110) and (001) susceptibilities probably results from differences in the Van Vleck susceptibility and anisotropy in the g factor.[10,11] When there exist two transitions, the difference between the high-H susceptibility and $\chi_{\min}$ for the (100) direction must correspond to $2(\chi_{\perp\perp}-\chi_{\parallel\parallel})$. In addition to the Van Vleck contribution, which is of order 5×10^{-8} cm^3/g for La_2CuO_4,[10] the measured susceptibilities also contain the diamagnetic core susceptibility, $\chi_d\sim-3.3\times10^{-7}$ cm^3/g.[12] As we show below, $2\chi_{\perp\perp}\approx4\times10^{-7}$ cm^3/g. Thus, the sum of all these contributions implies that $\chi^{110}\approx\chi_{\mathrm{II}}$. The solid curve in Fig. 5 represents results for Monte Carlo simulations of the $S=1/2$ SLQHA.[13] As discussed previously,[9] the magnitude and temperature dependence of the susceptibility are well described by the model 2D $S=1/2$ SLQHA if the antiferromagnetic exchange between nearest-neighbor CuII's is chosen to be $J_{\mathrm{II}}=10$ meV. The Néel ordering of the CuII's is made manifest by the cusp in the susceptibility at $T_{\mathrm{II}}=40\pm1$ K. One sees in Fig. 5 that, at low T and low H, χ is approximately two times larger in the (110) than in the (100) direction.

As seen in Fig. 6, below T_{II} the field dependence of M for the (110) direction is very similar to that at higher T (Fig. 3), but it is very different for the (100) direction. For (100), although the moment extrapolated to $H=0$ from high field still vanishes within the errors, $M(H)$ is now sigmoidal. This is demonstrated in Fig. 7, which shows $\chi(H)$ for the (100) direction for 200, 50, and 10 K. At low T the minimum value of χ occurs at $H=0$. Using the same arguments as for $T>T_{\mathrm{II}}$, we conclude that (110) is still the easy direction, with now *both* the staggererd moments of CuI and CuII perpendicular to the field, i.e., parallel to each other. The only difference here is that now χ_{II} should be replaced by $\chi_{\mathrm{II}\perp}$. As indicated in Figs. 5 and 7, the difference between the low and high H susceptibilities for the (100) direction is much larger at low T. Since the minimum of χ occurs at $H=0$, and since at this field the moments tend to point in the (110) direction, we conclude that for small fields in the (100) direction we have domains in which the moments are at 45° with the field, implying that in this region $\chi\approx(\chi_{\mathrm{II}\perp}+\chi_{\mathrm{II}\|}+2\chi_{\perp\perp}+2\chi_{\mathrm{I}\|})/2\approx\chi^{110}/2$. Also, we expect a permanent moment of magnitude $M_S^{110}/\sqrt{2}$ along the field, which agrees with the data shown in Fig. 8(a). Again, all of these features are explained by our theory, presented in Sec. V.

The T dependence of the permanent moment suggests that it is proportional to the antiferromagnetic order parameter. In Fig. 8(a) we plot the moment M_S^{110}. A fit to these data near T_{I} of the form $M_S^{110}\sim(T_{\mathrm{I}}-T)^{\beta}$ gives $\beta=0.27\pm0.03$ and $T_{\mathrm{I}}=(382\pm2)$ K; the solid curve is the fit. Figure 8(b) shows

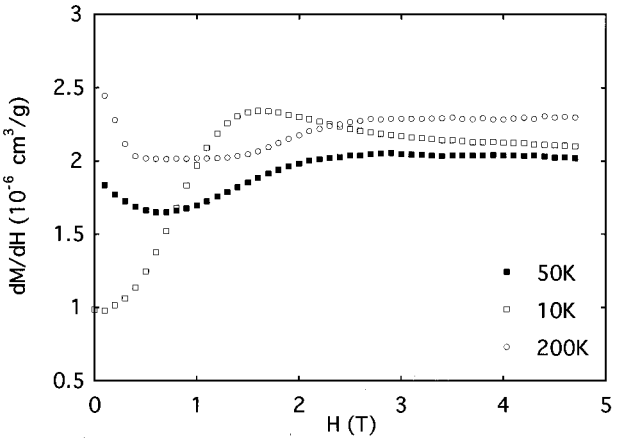

FIG. 7. dM/dH vs H for $\mathbf{H}\|(100)$ for temperatures above and below T_{II}.

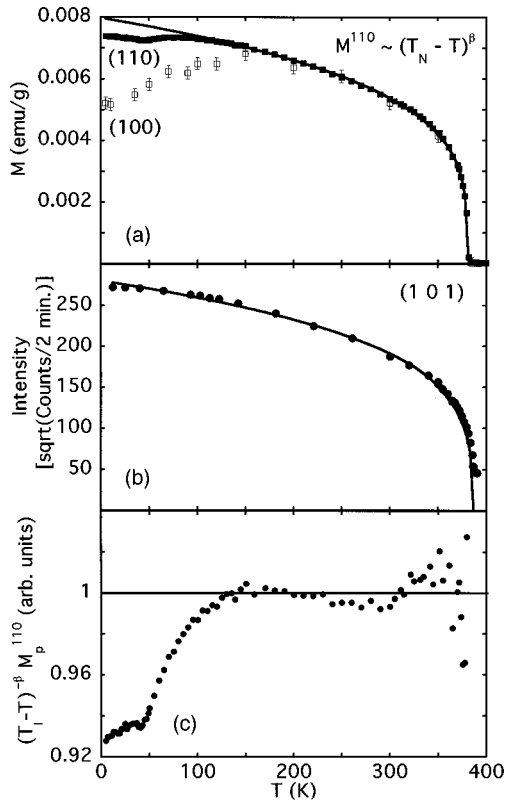

FIG. 8. (a) The permanent moment M_S^{110} vs T. (b) Square root of the antiferromagnetic Bragg peak intensity, proportional to the antiferromagnetic order parameter of the CuI's. The solid curves in (a) and (b) are power laws $\sim(T_{N,I}-T)^\beta$ with the same exponent to within experimental error. (c) Ratio of the permanent moment to the power law that describes the order parameter.

the intensity of the (101) Bragg peak, proportional to $(\boldsymbol{M}_\mathrm{I}^\dagger)^2$, and the solid curve is a fit to the form $(T_\mathrm{I}-T)^{2\beta}$.[14] The values of β determined by the two experiments are the same to within experimental error. The larger crystal used for the neutron measurements apparently has a slightly higher T_I than the crystal used for magnetization measurements. We plot the ratio $M_S^{110}/M_\mathrm{I}^\dagger$ in Fig. 8(c), using $(T_\mathrm{I}-T)^{0.27}$ for the order parameter.

IV. THEORY OF THE SPIN ROTATION TRANSITIONS FOR $T_\mathrm{II}<T<T_\mathrm{I}$

The temperature dependence of M_p suggests that there is a bilinear coupling between the observed ferromagnetic moment and the antiferromagnetic moment of the CuI subsystem. The Dzyaloshinsky-Moriya interaction generates such a coupling on each bond, but the average of this interaction vanishes by symmetry, as mentioned above. Furthermore, the latter interaction, when allowed, generates a permanent moment which does not vanish at high field for any field direction. The unusual field dependence of the magnetization and susceptibility (Figs. 3 and 4) result, instead, from a pseudodipolar coupling between the CuI system and the CuII system, as discussed below.[9] Since the ordering of the CuII spins makes the situation more complicated, we first discuss the behavior of the system for $T_\mathrm{II}<T<T_\mathrm{I}$. As discussed by Chou *et al.*,[9] the most general form of the interaction between a CuI and a neighboring CuII is

$$\mathcal{H}_{\mathrm{I\text{-}II}}=J^{\parallel}S_\mathrm{I}^{\parallel}S_\mathrm{II}^{\parallel}+J^{\perp}S_\mathrm{I}^{\perp}S_\mathrm{II}^{\perp}+J^{z}S_\mathrm{I}^{z}S_\mathrm{II}^{z}, \tag{1}$$

where $\parallel$ and $\perp$ denote parallel and perpendicular to the CuI-CuII bond.[15] We label the CuI's displaced from a central CuII in the directions $\hat{x},\hat{y},-\hat{x}$, and $-\hat{y}$, by 1,2,3, and 4, respectively. From neutron measurements[14] we know that the CuI spins are restricted to lie in the x-y plane. Summing over the four CuI-CuII bonds yields

$$\begin{aligned}\sum_{\text{bonds}}\mathcal{H}_{\mathrm{I\text{-}II}}&=J^{\parallel}(S_1^x+S_3^x)S_\mathrm{II}^x+J^{\perp}(S_1^y+S_3^y)S_\mathrm{II}^y\\&\quad+J^{\perp}(S_2^x+S_4^x)S_\mathrm{II}^x+J^{\parallel}(S_2^y+S_4^y)S_\mathrm{II}^y\\&=4[J_{\mathrm{av}}(\mathbf{S}_\mathrm{II}\cdot\mathbf{M}_\mathrm{I})+J_{\mathrm{pd}}(M_\mathrm{I}^{\dagger x}S_\mathrm{II}^x-M_\mathrm{I}^{\dagger y}S_\mathrm{II}^y)]\\&=4\mathbf{M}_\mathrm{II}\cdot(J_{\mathrm{av}}\mathbf{M}_\mathrm{I}+J_{\mathrm{pd}}\hat{\Gamma}\mathbf{M}_\mathrm{I}^\dagger),\end{aligned} \tag{2}$$

where $\mathbf{M}_\mathrm{I}=\Sigma_{i=1}^4\mathbf{S}_i/4$ and $\mathbf{M}_\mathrm{I}^\dagger=(\mathbf{S}_1+\mathbf{S}_3-\mathbf{S}_2-\mathbf{S}_4)/4$ denote the local uniform (ferromagnetic) and staggered moments of the CuI sublattice, $\mathbf{M}_\mathrm{II}=\mathbf{S}_\mathrm{II}$, and

$$J_{\mathrm{av}}=\frac{1}{2}(J^{\parallel}+J^{\perp}),\quad J_{\mathrm{pd}}=\frac{1}{2}(J^{\parallel}-J^{\perp}). \tag{3}$$

In Eq. (2) $\hat{\Gamma}\equiv\sigma_z$ is the 2×2 Pauli matrix which rotates (x,y) into $(x,-y)$, that is, $\hat{\Gamma}(x,y)\equiv(x,-y)$. It is clear from Eq. (2) that, in addition to the isotropic average exchange J_{av}, the term involving J_{pd} represents an *anisotropic* net interaction. It has the same symmetry as the dipolar field at the center of the plaquette from four magnetic point dipoles at the CuI sites. This term represents a bilinear coupling between $\mathbf{M}_\mathrm{I}^\dagger$ and $\mathbf{M}_\mathrm{II}$. Therefore, when $\mathbf{M}_\mathrm{I}^\dagger$ orders below T_I, it generates a net field $-4J_{\mathrm{pd}}\hat{\Gamma}\mathbf{M}_\mathrm{I}^\dagger$ on the CuII in the center of each plaquette. Since the CuII's occupy only every second plaquette, they are all surrounded by exactly the same configuration of CuI moments in each plane. Neutron measurements confirm that nearest-neighbor CuI's in adjacent planes order antiferromagnetically, as expected from the structure.[14] Because the plaquettes occupied by CuII's are staggered in adjacent planes, the CuII's in all planes see exactly the *same* local field and have the same ferromagnetic moment [Figs. 1(a)–1(c)].

In the theory we use dimensionless moments S and M, and measure the various J's, H and $1/\chi$ in ergs or eV. To translate into the experimental units of emu/g and cm^3/g, one needs to multiply M by $g\mu_B/m_{uc}=22.4$ emu/g, where $g=2$ and $m_{uc}=500\ g/N_A=83\times10^{-23}$ g, and χ by $(g\mu_B)^2/m_{uc}=4.16\times10^{-19}$ erg cm^3/g. Using $g=2.2$ will modify some of the parameters slightly.

To analyze the situation further, assume that $\mathbf{M}_\mathrm{I}^\dagger$ makes an angle θ with the x axis. Then $\mathbf{M}_\mathrm{I}^\dagger\equiv M_\mathrm{I}^\dagger(\cos\theta,\sin\theta)$, the last term in Eq. (2) is minimized when $\mathbf{M}_\mathrm{II}\|\hat{\Gamma}\mathbf{M}_\mathrm{I}^\dagger=M_\mathrm{I}^\dagger(\cos\theta,-\sin\theta)$, and the energy of this term is the same for all θ. In particular, the cases $\theta=-\pi/4,0$, and $-\pi/2$, shown in Figs. 1(a)–1(c) respectively, have the same energy, which is the minimum of this term for $J_{\mathrm{pd}}<0$. Thus the pseudodipolar interaction polarizes the CuII's in the directions shown by the dashed arrows in Figs. 1(a)–1(c).

Because of this polarization one has $\mathbf{M}_\mathrm{II}\neq0$, and the first term then generates a small ferromagnetic moment $\mathbf{M}_\mathrm{I}\|\mathbf{M}_\mathrm{II}$.

However, $\mathbf{M}_{\mathrm{I}}$ will be larger in the configuration of Fig. 1(a) than in that of Fig. 1(b), and the energy will consequently be lower. As usual, one has $\chi_{\mathrm{I}\perp} > \chi_{\mathrm{I}\parallel}$, because even at low T canting is possible when $\mathbf{M}_I \perp \mathbf{M}_I^{\dagger}$. Thus, the anisotropy of the CuI susceptibility gives rise to a fourfold symmetry, which prefers ordering of $\mathbf{M}_{\mathrm{II}}$ along (110), as indeed observed experimentally at low H.

However, we find that the first term in Eq. (2) is inadequate to account for the anisotropy we observe. An additional fourfold anisotropy energy, of the form $\mathcal{H}_4 = K\cos 4\theta = K(1-2\sin^2 2\theta)$, with $K>0$, which also prefers ordering along (110), has been shown to arise from quantum fluctuations for the CuI's in other cuprates.[15] Such an anisotropy does not arise as a single ion term for $S=1/2$. Our quantitative fits to the data require adding $\mathcal{H}_4$ to the Hamiltonian, with K close to the value predicted in Ref. 15. As discussed below, a field in the (100) direction competes with these anisotropies resulting in transitions from Fig. 1(a) to 1(b) to 1(c).

The anisotropic interactions in Eq. (1) could result from the usual dipole-dipole coupling. For the nearest-neighbor CuI-CuII interactions, this yields $J^{\parallel} = -2J^{\perp} = -2(g\mu_B)^2/r^3 \approx -20\ \mu$eV, where $r = a/2$ is the CuI-CuII bond length. Note that this gives $J_{\mathrm{pd}} < 0$. However, similar anisotropic terms may arise from direct or superexchange interactions involving spin-orbit and Coulomb exchange interactions, and these sometimes yield $J_{\mathrm{pd}} > 0$. In this case the polarization of the CuII's would point in the opposite direction to that indicated in Fig. 1.[15] Because of these other sources of the anisotropy with the same dipolar symmetry, we call the last term in Eq. (2) pseudodipolar. A measurement of the relative directions of the spins would identify the sign of J_{pd}.[16]

In the presence of an external field $\mathbf{H}$, Eq. (2) becomes

$$\mathcal{H} = -2\mathbf{H}\cdot\mathbf{M}_{\mathrm{I}} - \mathbf{H}_{\mathrm{II}}\cdot\mathbf{M}_{\mathrm{II}}, \tag{4}$$

with $\mathbf{H}_{\mathrm{II}} = \mathbf{H} - 4J_{\mathrm{av}}\mathbf{M}_I - 4J_{\mathrm{pd}}\hat{\Gamma}\mathbf{M}_I^{\dagger}$. (The factor 2 is the number of CuI's per planar unit cell, which contains one CuII.) Below T_{I}, both M_{I} and M_{II} turn out to be very small compared to $M_{\mathrm{I}}^{\dagger}$, and the magnitude of $M_{\mathrm{I}}^{\dagger}$ is practically not affected by the magnetic field. We therefore assume that this magnitude is constant, and expand the free energy per unit cell to quadratic order in the ferromagnetic moments

$$F = M_{\mathrm{I}\parallel}^2/\chi_{\mathrm{I}\parallel} + M_{\mathrm{I}\perp}^2/\chi_{\mathrm{I}\perp} + \mathbf{M}_{\mathrm{II}}^2/(2\chi_{\mathrm{II}}) - 2\mathbf{H}\cdot\mathbf{M}_{\mathrm{I}} - \mathbf{H}_{\mathrm{II}}\cdot\mathbf{M}_{\mathrm{II}} + \mathcal{H}_4. \tag{5}$$

This expression assumes isotropy of the CuII moment response, as appropriate for $T > T_{\mathrm{II}}$. We shall return to the case $T < T_{\mathrm{II}}$ in the next section. Minimizing with respect to $\mathbf{M}_{\mathrm{II}}$ now yields the usual linear response $\mathbf{M}_{\mathrm{II}} = \chi_{\mathrm{II}}\mathbf{H}_{\mathrm{II}}$, and substitution back in Eq. (5) then yields

$$F = M_{\mathrm{I}\parallel}^2/\tilde{\chi}_{\mathrm{I}\parallel} + M_{\mathrm{I}\perp}^2/\tilde{\chi}_{\mathrm{I}\perp} - \frac{1}{2}\chi_{\mathrm{II}}H^2 - 2\mathbf{H}_{\mathrm{I}}\cdot\mathbf{M}_{\mathrm{I}} + 4J_{\mathrm{pd}}\chi_{\mathrm{II}}\mathbf{H}\cdot\hat{\Gamma}\mathbf{M}_{\mathrm{I}}^{\dagger} + \mathcal{H}_4, \tag{6}$$

where $\mathbf{H}_{\mathrm{I}} = \mu\mathbf{H} + 8\chi_{\mathrm{II}}J_{\mathrm{av}}J_{\mathrm{pd}}\hat{\Gamma}\mathbf{M}_{\mathrm{I}}^{\dagger}$, $\mu = (1-2\chi_{\mathrm{II}}J_{\mathrm{av}})$, and

$$\tilde{\chi}_{\mathrm{I}\parallel} = \chi_{\mathrm{I}\parallel}/(1-8\chi_{\mathrm{II}}\chi_{\mathrm{I}\parallel}J_{\mathrm{av}}^2),$$

$$\tilde{\chi}_{\mathrm{I}\perp} = \chi_{\mathrm{I}\perp}/(1-8\chi_{\mathrm{II}}\chi_{\mathrm{I}\perp}J_{\mathrm{av}}^2). \tag{7}$$

Upon minimization with respect to $\mathbf{M}_{\mathrm{I}}$, F becomes

$$F = -\tilde{\chi}_{\mathrm{I}\parallel}H_{\mathrm{I}\parallel}^2 - \tilde{\chi}_{\mathrm{I}\perp}H_{\mathrm{I}\perp}^2 - \frac{1}{2}\chi_{\mathrm{II}}H^2 + 4J_{\mathrm{pd}}\chi_{\mathrm{II}}\mathbf{H}\cdot\hat{\Gamma}\mathbf{M}_{\mathrm{I}}^{\dagger} + \mathcal{H}_4. \tag{8}$$

To proceed we call the angle between the applied field and the $\hat{x}$ direction α, so that $H_{\parallel} = H\cos(\theta-\alpha)$, $H_{\perp} = H\sin(\theta-\alpha)$. Using also $(\hat{\Gamma}\mathbf{M}_{\mathrm{I}}^{\dagger})_{\parallel} = M_{\mathrm{I}}^{\dagger}\cos 2\theta$, $(\hat{\Gamma}\mathbf{M}_{\mathrm{I}}^{\dagger})_{\perp} = M_{\mathrm{I}}^{\dagger}\sin 2\theta$, we end up (apart from a constant) with

$$F(\theta) = -[\chi_{\mathrm{II}} + 2\mu^2\tilde{\chi}_{\mathrm{I}\parallel} + 2\mu^2\Delta\chi\sin^2(\theta-\alpha)]H^2/2 + M_0H[(1-4\tilde{\chi}_{\mathrm{I}\parallel}\mu J_{\mathrm{av}})\cos(\theta+\alpha) - 4J_{\mathrm{av}}\mu\Delta\chi\sin 2\theta\sin(\theta-\alpha)] - k\sin^2 2\theta, \tag{9}$$

where $M_0 = 4J_{\mathrm{pd}}\chi_{\mathrm{II}}M_{\mathrm{I}}^{\dagger}$, $\Delta\chi = \tilde{\chi}_{\mathrm{I}\perp} - \tilde{\chi}_{\mathrm{I}\parallel}$ and $k = 2K + 4M_0^2J_{\mathrm{av}}^2\Delta\chi$. At low temperatures, $\chi_{\mathrm{I}\parallel} \ll \chi_{\mathrm{I}\perp} \approx 0.53/(8J_0)$, where J_0 is the CuI-CuI exchange energy and the factor of 0.53 comes from quantum corrections.[17,13] Neglecting $\chi_{\mathrm{I}\parallel}$ then yields the low-T approximation used in Ref. 9 to fit our data.

Setting $\partial E/\partial\theta = 0$ gives an equation for $\theta(H)$:

$$\mu^2\Delta\chi H^2\sin 2(\theta-\alpha) + M_0H[(1-4\mu\tilde{\chi}_{\mathrm{I}\parallel}J_{\mathrm{av}})\sin(\theta+\alpha) + 4\mu J_{\mathrm{av}}\Delta\chi[2\cos 2\theta\sin(\theta-\alpha) + \sin 2\theta\cos(\theta-\alpha)] + 2k\sin 4\theta = 0. \tag{10}$$

Having solved this equation for θ, one finds the magnetic moment to be

$$M = -\partial E/\partial H = [\chi_{\mathrm{II}} + 2\mu^2\tilde{\chi}_{\mathrm{I}\parallel} + 2\mu^2\Delta\chi\sin^2(\theta-\alpha)]H - M_0[(1-4\tilde{\chi}_{\mathrm{I}\parallel}\mu J_{\mathrm{av}})\cos(\theta+\alpha) - 4J_{\mathrm{av}}\mu\Delta\chi\sin 2\theta\sin(\theta-\alpha)]. \tag{11}$$

In practice, we find it more convenient to use θ as a parameter, then solve the quadratic Eq. (10) for H and thus get $H(\theta)$ and $M(\theta)$ parametrically. Equations (10), (11) contain six material parameters χ_{II}, $\chi_{\mathrm{I}\parallel}$, $\chi_{\mathrm{I}\perp}$, M_0, J_{av}, and k. We also treat α as a parameter because the alignment of the crystal axes with the magnetic field is accurate to only a degree or two in our sample holder. The resulting fits show that the accuracy in α is about 0.2° to 0.4°. Our procedure for determining these parameters is as follows: If it were true that $\alpha = \pi/4$, precisely, for the data labeled (110) and $\alpha = 0$, precisely, for that labeled (100), then the parameters M_S^{110}, M_S^{100}, χ^{110}, and χ^{100} could be determined in a straightforward way. When $\alpha = \pi/4$, the minimum of $F(\theta)$ is given by $\theta = \pi/4 + \mathrm{sgn}(J_{\mathrm{pd}})\pi/2$ for all H. That is, configuration 1(a) is always the ground state for $J_{\mathrm{pd}} < 0$. Substituting these values in Eq. (11) we find

$$M_S^{110} = |M_0|(1-4J_{\mathrm{av}}\mu\tilde{\chi}_{\mathrm{I}\perp}),$$

$$\chi^{110}=\chi_{\mathrm{II}}+2\mu^2\tilde{\chi}_{\mathrm{I}\perp}. \tag{12}$$

When $\alpha=0$, then Eq. (10) has two types of solutions: either $\sin\theta=0$ or $x=\cos\theta$ must be a solution of the cubic equation

$$H^2\mu^2\Delta\chi x+M_0H[1-4\mu\tilde{\chi}_{\mathrm{I}\parallel}J_{\mathrm{av}} +8J_{\mathrm{av}}\mu\Delta\chi(3x^2-1)]/2+4k(2x^3-x)=0. \tag{13}$$

For certain ranges of the parameters, this cubic equation has no real solutions with $|x|\leqslant 1$. This happens for $H_{c1}<H<H_{c2}$, where H_{c1} and H_{c2} are the solutions of the quadratic equation obtained from Eq. (13) by setting $x=-\mathrm{sgn}(J_{\mathrm{pd}})$. Apparently, this quadratic equation has real positive solutions for $H_{c1,2}$ only at $T>150$ K. In the range between these two critical fields, the only admissible solution has $\sin\theta=0$, corresponding to the structure in Fig. 1(b). Setting $\alpha=\theta=0$ in Eq. (11) we then have a straight $M(H)$, with

$$M_S^{100}=|M_0|(1-4J_{\mathrm{av}}\mu\tilde{\chi}_{\mathrm{I}\parallel}),$$

$$\chi^{100}=\chi_{\mathrm{II}}+2\mu^2\tilde{\chi}_{\mathrm{I}\parallel}. \tag{14}$$

Although $\sin\theta=0$ is always an extremum of $F(\theta)$, it represents the minimum only for $H_{c1}<H<H_{c2}$. Outside of this range the minimum is given by the solution to Eq. (13), which varies with H: $|\cos\theta|$ starts at $\sqrt{2}/2$ for $H=0$ [yielding the structure in Fig. 1(a) for $J_{\mathrm{pd}}<0$], increases towards 1 at $H=H_{c1}$, where it remains up to H_{c2}, corresponding to Fig. 1(b), and decreases towards 0 [i.e., Fig. 1(c)] as $H\to\infty$ above H_{c2}. This reproduces our data at 200 K, and relates them to the spin rotations between Figs. 1(a)–1(c). For all $\alpha\neq 0$, and also when the solutions $H_{c1,2}$ do not exist (as happens at lower T), the solution $\sin\theta=0$ does not apply, the sharp transitions disappear, and there is only one continuous solution for θ. As seen in Fig. 4, the critical fields are not observed at temperatures below about 150 K. This probably happens because $\Delta\chi$ grows as T decreases, so that eventually the quadratic equation loses its real roots.

For very large H, the value of θ found from Eq. (10) follows $\theta-\alpha\approx\mathrm{sgn}(J_{\mathrm{pd}})\pi/2+\mathcal{O}(1/H)$, and substituting this into Eq. (11) gives

$$M=\chi^{110}H+M_S^{110}\sin 2\alpha+\mathcal{O}(1/H), \tag{15}$$

consistent with the parallel asymptotes in Fig. 3. In this limit, $\mathbf{M}_{\mathrm{I}}^{\dagger}\perp\mathbf{H}$ [e.g., Fig. 1(c)], taking advantage of $\chi_{\mathrm{I}\perp}>\chi_{\mathrm{I}\parallel}$.

To compare theory with experiment for all the data we find it useful to emphasize the deviations of $M(H)$ from $\chi^{110}H$, using the quantity

$$m(H,\alpha)=(M-\chi^{110}H)/M_S^{110}. \tag{16}$$

Our procedure is as follows: For each T, M_S^{110} is found from measurements in the (110) direction. For each data set χ^{110} is determined by insisting that m approaches a constant for high H [see Eq. (15)]. This constant should in fact be equal to $\sin 2\alpha$. Thus, χ^{110} can also be determined from data for the (100) direction. This is very sensitive, and we are satisfied to note that our (100) data give values close to those for the (110) data at the same temperature. The differences may result from variations in alignment which introduce various amounts of the higher (001) susceptibility. We then carry out a least-squares fit of Eq. (16) to the data. For 200 K, when we have the two transitions, we use Eqs. (12) and (14) to estimate the parameters M_S^{110}, M_S^{100}, χ^{110} and χ^{100}. It is now useful to note that Eq. (9) can be written in the form

$$F=-[\chi^{100}\cos^2(\theta-\alpha)+\chi^{110}\sin^2(\theta-\alpha)]H^2/2 +\mathrm{sgn}(J_{\mathrm{pd}})H[M_S^{100}\cos(\theta-\alpha)\cos 2\theta +M_S^{110}\sin(\theta-\alpha)\sin 2\theta]-k\sin^2 2\theta. \tag{17}$$

Equation (11) thus becomes

$$M=H[\chi^{100}\cos^2(\theta-\alpha)+\chi^{110}\sin^2(\theta-\alpha)]-\mathrm{sgn}(J_{\mathrm{pd}}) \times[M_S^{100}\cos(\theta-\alpha)\cos 2\theta+M_S^{110}\sin(\theta-\alpha)\sin 2\theta]. \tag{18}$$

This equation has a simple interpretation, along the lines discussed qualitatively in Sec. III: The first term contains an average of the parallel and longitudinal susceptibilities, with the appropriate projections of the field onto these directions. The second term contains the effect of the internal field $\mathbf{H}_{\mathrm{pd}}=-4J_{\mathrm{pd}}\hat{\mathbf{\Gamma}}\mathbf{M}_{\mathrm{I}}^{\dagger}$ on the CuII; this field generates components $M_{\mathrm{II}\parallel,\perp}=\chi_{\mathrm{II}\parallel,\perp}H_{\mathrm{pd}\parallel,\perp}$, and the projection of this moment in the direction of the field gives the residual permanent moment in the second term of Eq. (18). Substituting in Eq. (16) now yields

$$m=-A\cos^2(\theta-\alpha)-\mathrm{sgn}(J_{\mathrm{pd}}) \times[B\cos(\theta-\alpha)\cos 2\theta+\sin(\theta-\alpha)\cos 2\theta], \tag{19}$$

with $A=(\chi^{110}-\chi^{100})/M_S^{110}$ and $B=M_S^{100}/M_S^{110}$. The equation for θ now has the form

$$H^2A\sin 2(\theta-\alpha)-2\mathrm{sgn}(J_{\mathrm{pd}})H[(2-B)\sin(\theta-\alpha)\cos 2\theta +(1-2B)\cos(\theta-\alpha)\sin 2\theta]+C\sin 4\theta=0, \tag{20}$$

with $C=4k/M_S^{110}$. Therefore, the data for m can be used to fit the four parameters A, B, C, and α. In practice, for $T>150$ K we start with the values of M_S^{110}, M_S^{100}, χ^{110}, and χ^{100} which are estimated from measurements with fields along (110) and (100), and then refine their values by fitting Eqs. (19) and (20). The parameters do not change much during the fitting procedure. For temperatures below 150 K, for which there are no critical fields, there have been difficulties with convergence of the least-squares algorithm. We therefore begin with the parameters at higher T and vary them slightly, recalculating $m(H)$ until a good fit is obtained. Figure 9 shows the results of this fitting procedure for three temperatures. For $T<150$ K we find no magnetic field for which $\theta=0$. This is consistent with the absence of a region of constant χ^{100} in Fig. 4 at low T.

As discussed previously,[9] when we neglect $\chi_{\mathrm{I}\parallel}$ and use $M_{\mathrm{I}}^{\dagger}\approx 0.3$ and $\chi_{\mathrm{I}\perp}\approx 0.53/(8J_0)$ then the data below 120 K can all be fitted with $J_{\mathrm{av}}=-(12\pm 9)$ meV, $J_0=(130\pm 40)$ meV, $|J_{\mathrm{pd}}|=(27\pm 1)$ μeV, $K=(10\pm 3)\times 10^{-7}$ meV. At higher T the parameters are somewhat different as expected.[9] In particular, the decrease of anisotropy of the CuI susceptibility means that $\Delta\chi$ decreases as T_{I} is approached. This increases the range of stability of the phase in Fig. 1(b). It is

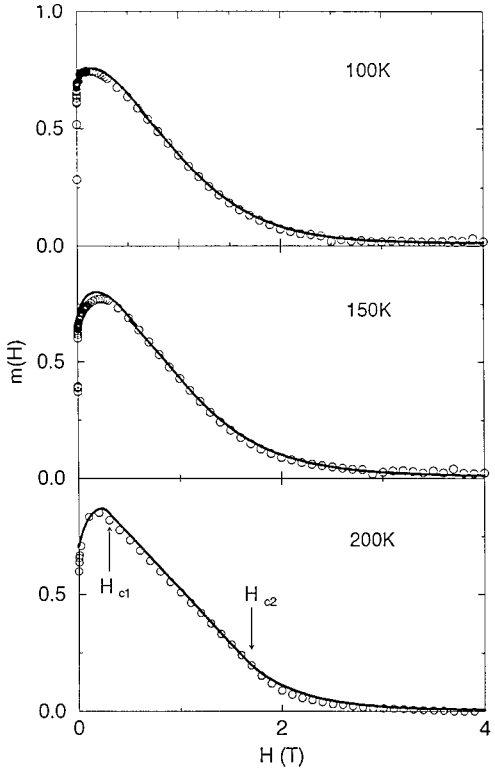

FIG. 9. Theoretical (full lines) and measured values of $m(H,\alpha=0)$ for three temperatures. At 200 K the two spin rotation fields are identified.

interesting to note that our measurements imply a decrease of $\Delta\chi$ by about 70%. This decrease is close to that observed in MnF_2 when T/T_N increases from about 0.26 to about 0.52.[18]

V. THEORY BELOW T_{II}

As mentioned, the data for **H** along (110) indicate that the staggered moments of CuI and CuII tend to be perpendicular to the field and parallel to each other. This tendency is understandable even on the basis of the theory presented so far: Staggered moments are more likely to be perpendicular to ferromagnetic moments on the same Cu ions. However, we now argue that this tendency also exists in the absence of the ferromagnetic moment, due to fluctuations about the *average* coupling between the staggered moments of the CuI and CuII. If one includes such fluctuations, and treats them perturbatively, then one generates a new term in the energy, which prefers collinearity of these staggered moments.[19] In our effective mean field approach, this can be written in the form

$$E_{\rm col}=-A(\mathbf{M}_{\rm I}^{\dagger}\cdot\mathbf{M}_{\rm II}^{\dagger})^2, \tag{21}$$

where $A\sim J_{\rm av}^2/J_0\sim 1$ meV. It should be noted that both this term and the internal field $-4J_{\rm pd}\hat{\Gamma}\mathbf{M}_{\rm I}^{\dagger}$ which acts on the CuII imply a uniaxial anisotropy α, so that the CuII ordering is prefered along the (110) direction. This is the reason why the critical behavior of the transition at $T_{\rm II}$ is that of the two-dimensional Ising model. These terms also imply a gap in the spin wave spectrum, consistent with our neutron scattering results. The value of that gap is also consistent with

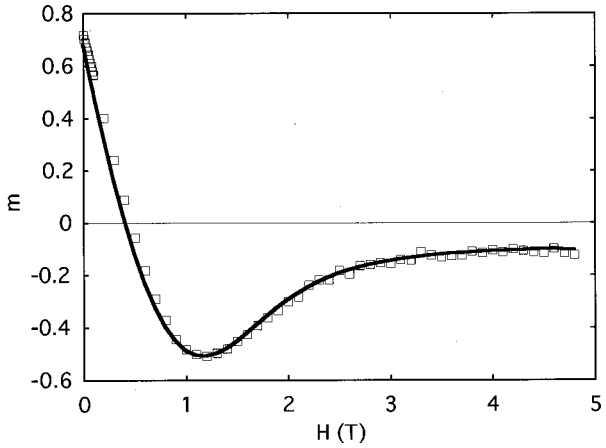

FIG. 10. Same as Fig. 9 for $T=10$ K.

the value of $T_{\rm II}$, as deduced from the approximate relation $\alpha\xi^2\sim 1$, where ξ is the correlation length of the planar Heisenberg model.[14]

The other main modification of the theory presented above results from the ordering of the CuII's. This implies that the term $\mathbf{M}_{\rm II}^2/(2\chi_{\rm II})$ in Eq. (5) must now be replaced by $M_{\rm II\|}^2/(2\chi_{\rm II\|})+M_{\rm II\perp}^2/(2\chi_{\rm II\perp})$, where $\|$ and $\perp$ now relate to $\mathbf{M}_{\rm II}^{\dagger}$. We thus minimize

$$F=M_{\rm I\|}^2/\chi_{\rm I\|}+M_{\rm I\perp}^2/\chi_{\rm I\perp}+M_{\rm II\|}^2/(2\chi_{\rm II\|})+M_{\rm II\perp}^2/(2\chi_{\rm II\perp})-2\mathbf{H}\cdot\mathbf{M}_{\rm I}-\mathbf{H}_{\rm II}\cdot\mathbf{M}_{\rm II}+E_{\rm col}+\mathcal{H}_4. \tag{22}$$

Our estimates show that below $T_{\rm II}$, $E_{\rm col}$ is much larger than K and other anisotropies. Therefore, we now simplify the analysis by adding the constraint that $\mathbf{M}_{\rm II}^{\dagger}$ always remains parallel to $\mathbf{M}_{\rm I}^{\dagger}$. This again leaves only one angle θ to be found from the minimization. We can now repeat all the algebraic steps of the previous section, and we find that $F(\theta)$ has the same form as in Eq. (17), but with the new parameters

$$\chi^{110}=\chi_{\rm II\perp}+2\mu_{\perp}^2\tilde{\chi}_{\rm I\perp},$$

$$\chi^{100}=\chi_{\rm II\|}+2\mu_{\|}^2\tilde{\chi}_{\rm I\|},$$

$$M_S^{110}=4|J_{\rm pd}|\chi_{\rm I\perp}M_{\rm I}^{\dagger}(1-4\mu_{\perp}J_{\rm av}\tilde{\chi}_{\rm I\perp}),$$

$$M_S^{100}=4|J_{\rm pd}|\chi_{\rm II\|}M_{\rm I}^{\dagger}(1-4\mu_{\|}J_{\rm av}\tilde{\chi}_{\rm I\|}),$$

$$k=2K+8J_{\rm pd}^2(M_{\rm I}^{\dagger})^2[\chi_{\rm I\perp}/(1-8J_{\rm av}^2\chi_{\rm II\perp}\chi_{\rm I\perp})-\chi_{\rm II\|}/(1-8J_{\rm av}^2\chi_{\rm II\|}\chi_{\rm I\|})], \tag{23}$$

with $\mu_{\|,\perp}=1-2J_{\rm av}\chi_{\rm II\|,\perp}$. These expressions reduce to those of Sec. IV when one sets $\chi_{\rm II\|}=\chi_{\rm II\perp}=\chi_{\rm II}$. Qualitatively, note that now we have $\chi^{100}\ll\chi^{110}$, implying a much more anisotropic susceptibility, as indeed observed experimentally. Also, the contribution of the second term in k is now larger than before. We can now follow all the steps described following Eq. (17), and fit the data for $m(H)$. For **H** along (110), Fig. 6 gives $\chi^{110}\simeq 2.16\times10^{-6}$ cm^3/g and $M_S^{110}\simeq 0.00736$ emu/g. Figure 10 shows the function $m(H)$ obtained from using these values for the field along (100), together with a fit to Eqs. (19) and (20). In fact, the fit shows

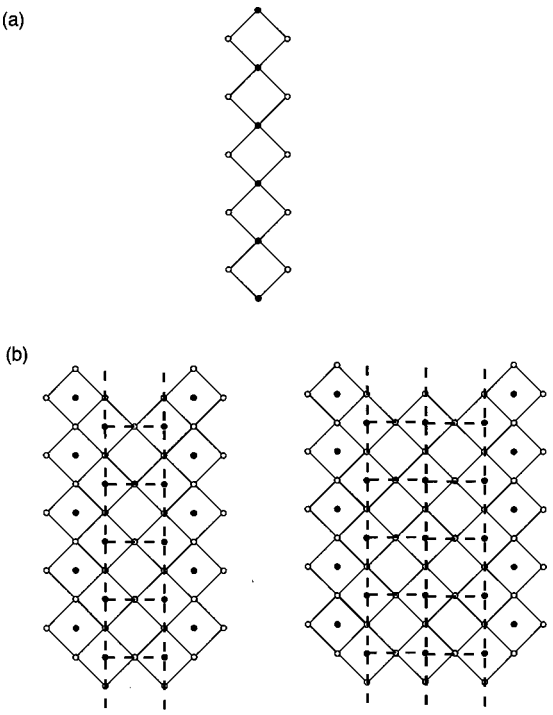

FIG. 11. (a) CuO_2 chain. (b) Two- and three-legged cuprate ladders.

that the experiment had $\alpha=-(2.6\pm0.3)°$. The fit yields the parameters $A=(3.5\pm0.2)\ \mathrm{T}^{-1}$, $B=0.16\pm0.03$, and $C=(1.9\pm0.1)$ T. We can now compare these values with those given by our theory. Using the parameters cited at the end of the previous section, together with $\chi_{\mathrm{II}\perp}\approx0.53/(8J_{\mathrm{II}})\approx6.6\ \mathrm{eV}^{-1}$ and $\tilde{\chi}_{\mathrm{I}\perp}\approx\chi_{\mathrm{I}\perp}\approx0.53/(8J_0)\approx0.51\ \mathrm{eV}^{-1}$, and neglecting the parallel susceptibilities, we find $\chi^{110}\approx8\ \mathrm{eV}^{-1}=2.1\times10^{-6}\ \mathrm{cm}^3/\mathrm{g}$, in excellent agreement with the measured value. In contrast, if we use our earlier estimate $|J_{\mathrm{pd}}|\approx27\ \mu\mathrm{eV}$ then Eq. (23) now yields $M_S^{110}\approx0.0049$ emu/g, significantly smaller than the measured value. Figure 8(c) reveals an interesting question: To a good approximation, our theory predicts that the ratio $M_S^{110}/M_{\mathrm{I}}^{\dagger}$ should be proportional to $\chi_{\mathrm{II}\perp}$. In fact, this ratio varies much less than the susceptibility shown in Fig. 5. We have no explanation for this discrepancy.

The measured value of C can be used to extract $K\approx7.2\times10^{-6}$ meV, larger by a factor of about 7 than its value around 100 K. This large increase of the anisotropy parameter K with decreasing T is also unexplained. Finally, the fitted value of B implies that $\chi_{\mathrm{II}\parallel}/\chi_{\mathrm{II}\perp}\approx0.16$, somewhat larger but in rough agreement with the analogous results in MnF_2 for $T/T_N\sim1/4$.[18] Using this for an estimate of $\chi^{100}\approx\chi_{\mathrm{II}\parallel}$, we can then use A to estimate $M_S^{110}\approx0.0052$ emu/g, much closer to our theoretical estimate given above.

VI. IMPLICATIONS FOR OTHER SYSTEMS

As mentioned in the Introduction, there has been much recent interest in cuprates with chains and ladders.[2] In this section we explain how our measurements give direct information on the coupling constants in many of these systems.

Figure 11(a) shows the Cu chain which exists, e.g., in $Sr_{41}Cu_{24}O_{41}$.[20] Note that the nearest-neighbor Cu-Cu superexchange, mediated by the oxygen ion, has roughly the same 90° Cu-O-Cu geometry as our CuI-CuII coupling. Therefore, we predict that this coupling is anisotropic, with coupling constants $J^{\parallel}$ for spin components along the bond and $J^{\perp}$ for the perpendicular components. The fact that this coupling is mainly ferromagnetic has not been clear in the literature before. Furthermore, the next-nearest-neighbor superexchange in these chains has roughly the same Cu-O-O-Cu geometry as our nearest-neighbor CuII-CuII coupling. The large ratio of this next-nearest-neighbor exchange to the nearest-neighbor one can explain the finite gap observed in these spin 1/2 Heisenberg chains.[21] It would be interesting to study theoretically the effects of the Ising anisotropy (coming from the in-plane anisotropy together with J_{pd}) on this gap.

Assuming that the CuII-CuII superexchange results mainly from the Cu-O-O-Cu paths (and not from the CuII-CuI-CuII one), we observe that these paths are the same as those connecting the next-nearest-neighbor CuI's. These, in turn, appear in all the lamellar cuprates, e.g., in $Sr_2CuO_2Cl_2$. We thus estimate this next nearest neighbor exchange to be $J'\approx J_{\mathrm{II}}\approx10$ meV. It is rewarding to note that recent ARPES studies of this latter system indeed require an effective next nearest neighbor hopping energy $t'\approx t/3$, i.e., $J'/J_0\approx1/9$,[22] in rough agreement with our estimate.

Finally, Fig. 11(b) shows examples of two- and three-legged ladders, which exist in materials such as $Sr_{n-1}Cu_{n+1}O_{2n}$.[2] Clearly, the coupling between neighboring ladders (which are shifted by half a Cu-Cu distance) involves again the same 90° Cu-O-Cu superexchange coupling as for our CuI-CuII interaction. Thus, this coupling (which is also frustrated as in our case) would be dominated by our colinearity and by our pseudodipolar anisotropic coupling J_{pd}. The spin structures of such ladders in the direction perpendicular to the ladders (in the plane) should be determined by the competition between these interactions and other anisotropies. We should add that the different oxygen surroundings of copper pairs along and perpendicular to each ladder, combined with the bond-dependent anisotropies such as those discussed in the present paper, imply anisotropic exchange also for these bonds, with possibly different values for these two types of bonds. Such anisotropy should decrease the gap and increase the correlation length along the even-legged ladders, and might explain how they could develop two dimensional Ising-like long range order.

VII. DISCUSSION

The theory in Secs. IV and V describes the field dependence of the magnetization very well in both ordered phases. Not only does the theory explain the peculiar behavior of the moment and susceptibility seen in Figs. 3, 4, 6, and 7 for the (110) and (100) directions, but also it predicts the dependence on the angle α, as discussed by Chou *et al.*[9]

However several aspects are not yet understood. In particular, the theory predicts that $M_S^{110}=4J_{\mathrm{pd}}\chi_{\mathrm{II}}M_{\mathrm{I}}^{\dagger}$, while Fig. 8 shows that the ratio of M_S to $M_{\mathrm{I}}^{\dagger}$ does not have the same temperature dependence as $\chi^{100}=\chi_{\mathrm{II}}$. Indeed, except at the lowest temperatures, the ratio is independent of T suggesting that the induced moment on the CuII's saturates. A possible way to resolve this difficulty exists near T_{I}. There one could treat the problem using a Ginzburg-Landau-Wilson expan-

sion of the free energy density. Within such an approach, the order parameters $\mathbf{M}_{\mathrm{II}}$ and $\mathbf{M}_{\mathrm{I}}^{\dagger}$ would mix due to their bilinear coupling, yielding a constant ratio $J_{\mathrm{pd}}/2J_0$, instead of $4J_{\mathrm{pd}}\chi_{\mathrm{II}}$. The former ratio is also predicted at very low T, where χ_{II} is replaced by $\chi_{\mathrm{II}\perp}=1/8J_{\mathrm{II}}$. It is not clear how to extend this to intermediate temperatures.

The mixing of the two order parameters also implies a mixing of χ_{II} with the staggered susceptibility $\chi_{\mathrm{I}}^{\dagger}$, which diverges at T_{I}. [23] However, the temperature where this would be observed is apparently too narrow because of the small ratio of the divergent part to χ_{II}. More accurate measurements very close to T_{I} would be desirable.

ACKNOWLEDGMENTS

This work has been supported primarily by the MRSEC Program of the National Science Foundation under Grant No. DMR 94-00334 at MIT, the U. S.-Israel Binational Science Foundation (at Tel Aviv, MIT, and Penn), the Israel Science Foundation (at Tel Aviv), and the NSF Grant No. DMR-95-20175 (at Penn).

[1] M. Greven, R. J. Birgeneau, Y. Endoh, M. A. Kastner, M. Matsuda, and G. Shirane, Z. Phys. B **96**, 465 (1995).
[2] E. Dagotto and T. M. Rice, Science **271**, 618 (1996).
[3] B. Grande and H. Muller-Buschbaum, Z. Naturforsch. B **31**, 405 (1976).
[4] H. Müller-Buschbaum, Angew. Chem. Int. Ed. Engl. **16**, 674 (1977).
[5] K. Yamada, N. Suzuki, and J. Akimitsu, Physica B **213-214**, 191 (1995).
[6] S. Noro *et al.*, Mater. Sci. Eng., B **25**, 167 (1994).
[7] T. Ito *et al.* (unpublished).
[8] T. Ito, H. Yamaguchi, and K. Oka, Phys. Rev. B **55**, 684 (1997).
[9] F. C. Chou *et al.*, Phys. Rev. Lett. **78**, 535 (1997).
[10] D. C. Johnston, Phys. Rev. Lett. **62**, 957 (1989).
[11] D. Vaknin *et al.*, Phys. Rev. B **49**, 9057 (1994).
[12] P. Selwood, *Magnetochemistry* (Interscience, New York, 1956), p. 78.
[13] M. Greven, Ph.D. thesis, MIT, 1995.
[14] Y. J. Kim *et al.* (unpublished).
[15] T. Yildirim, A. B. Harris, O. Entin-Wohlman, and A. Aharony, Phys. Rev. Lett. **73**, 2919 (1994); **74**, 2843 (1995); T. Yildirim, A. B. Harris, A. Aharony, and O. Entin-Wohlman, Phys. Rev. B **52**, 10 239 (1995). The latter references contain the corrected estimate $K\approx 10^{-7}$ meV.
[16] Recent superexchange calculations indicate that the origin of J_{pd} is mainly dipolar [S. Tornow, A. Aharony, and O. Entin-Wohlman (unpublished)].
[17] M. Makivic and H.-Q. Ding, Phys. Rev. B **43**, 3562 (1991).
[18] C. Kittel, *Introduction to Solid State Physics*, 6th ed. (Wiley, New York, 1986), p. 447.
[19] E. F. Shender, Sov. Phys. JETP **56**, 178 (1982).
[20] M. Matsuda and K. Katsumata, Phys. Rev. B **53**, 12 201 (1996).
[21] G. Castilla, S. Chakravarty, and V. J. Emery, Phys. Rev. Lett. **75**, 1823 (1995).
[22] C. Kim *et al.* (unpublished).
[23] A similar singularity in χ occurs in La_2CuO_4, where the mixing comes from the Dzyaloshinsky-Moriya interaction [T. Thio, T. R. Thurston, N. W. Preyer, P. J. Picone, M. A. Kastner, H. P. Jenssen, D. R. Gabbe, C. Y. Chen, R. J. Birgeneau, and A. Aharony, Phys. Rev. B **38**, 905 (1988)].